TELKOMNIKA, Vol. 11, No. 2, February 2013, pp. 906~912
ISSN: 2302-4046

Study of High Indium $In_XGa_{1-X}N$ Alloys with Synchrotron Radiation

Wei Zheng[1,2,a], Zhe Chuan Feng[2,b], Rui Sheng Zheng[1,c], Hao-Hsiung Lin[2], Xin Qiang Wang[3], Ting-Shan Chan[4], Ling-Yun Jang[4], and Chee Wee Liu[2,5]

[1]Key Laboratmory of Optoelectronic Devices and Systems of Ministry of Education and Guangdong Province, Institute of Optoelectronics, Shenzhen University, Shenzhen, 518060, China
[2]Institute of Photonics & Optoelectronics, Department of Electrical Engineering, and Center for Emerging Material and Advanced Devices, National Taiwan University, Taipei, 106-17 Taiwan
[3]State Key Laboratory of Artificial Microstructure and Mesoscopic Physics, School of Physics, Peking University, Beijing, 100871 China
[4]National Synchrotron Radiation Research Center, Hsinchu, 30076, Taiwan
[5]National Nano Device Laboratories, Science-based Industrial Park, Hsinchu, 30078 Taiwan
*Corresponding author, e-mail: [a]zhengwei@email.szu.edu.cn, [b]fengzc@cc.ee.ntu.edu.tw, [c]rszheng@szu.edu.cn

Abstract

InGaN thin films with near entire indium composition range have been successfully grown on GaN/sapphire (0001) by molecular beam epitaxy (MBE). X-ray absorption fine structure have been used to study the local structure of some typical $In_xGa_{1-x}N$ alloys with high indium (In) composition of x=0.78 and 0.86. A detailed analysis of the extended x-ray absorption fine structure of In K-edge by using the IFEFFIT program, and the chemical bonds of In-N are obtained. The x-ray absorption near-edge structure of In K- and L-edge and N K-edge are investigated, and the electronic structure of $In_xGa_{1-x}N$ are determined with these high In content $In_xGa_{1-x}N$ ternary compounds. The calculated XANES spectra of N K-edge, based on first principle method, are consistent with the observed spectra.

Keywords: *EXAFS; XANES, $In_xGa_{1-x}N$, bond length, local structure formatting*

1. Introduction

InGaN semiconductor materials have been extensively investigated owing to their applications in light-emitting diodes, photo-detectors, laser diodes, and high-speed and high-power electronic devices. In recent years, a great deal of developments and breakthroughs have been achieved in III-nitride based materials and devices, including light emitting diodes (LEDs), laser diodes (LDs) and other wide range of electronic, optoelectronic and photonic devices [1-3]. Among them, InGaN or InGaN/GaN quantum well (QW) are usually employed as the active layers. The ternary alloy InGaN possesses the tunable direct band gap varying from 0.65 eV (InN) to 3.4 eV (GaN), i.e. covers a wide spectral range from infrared (IR) to visible and to ultraviolet (UV) [4-7]. For a long time, the energy gap of InN was considered to be about 1.95 eV [1, 8]. Only since ten years ago, it is corrected as 0.6-0.7 eV [9-12], which greatly expands the spectral range of InGaN. This makes the InGaN can serve for whole spectrum solar cells [13-15]. Intensive research has been carrying on InGaN in past years [4-25]. However, this ternary InGaN alloy (and other III-nitride ternary and quaternary alloys) is predicted to be thermodynamically unstable [26]. There exists a large difference in interatomic spacing between InN and GaN of about 11%, due to very different tetrahedral radii of the atomic species occupying different sublattices [4, 23], which can give rise to a solid miscibility and high strains. The resulting strain could lead to deviations from homogeneity of the sublattice. Two types of compositional inhomogeneity could occur: phase separation and atomic ordering. Phase separation is driven by strains due to the mixing of two mismatched lattices, while atomic ordering is caused by surface reconstruction and induced subsurface stress. The inside stress could force the preferential occupation of lattice sites by atomic species with different radii [4, 23].

Received September 3, 2012; Revised December 31, 2012; Accepted January 15, 2013

Above factors have leaded to the difficulties in growing high indium compositional InGaN epitaxial materials, which were limited to around or less than 35% of x(In) in $In_xGa_{1-x}N$ for years [4, 8, 16, 19, 23]. Great efforts in the growth of $In_xGa_{1-x}N$ with high x(In) or in full In-compositional range have been made in recent years [5, 7, 18, 20, 21, 24]. But, some epitaxial $In_xGa_{1-x}N$ materials with high x(In) are not so good, and it is still a big challenging for growing high quality of $In_xGa_{1-x}N$ materials with high x(In) or in full compositional range. For the growth of $In_xGa_{1-x}N$ with high x(In), metalorganic chemical vapor deposition (MOCVD) [5], molecular beam epitaxy (MBE) [18, 20] and some other technologies such as modified activated reactive evaporation (MARE) [7], metal-modulated epitaxy (MME) [21] and reactive radio-frequency magnetron sputtering [24], have been employed. Because of the low dissociation temperature of InGaN, the growth is favorable at low temperatures. For MOCVD, it uses ammonia or hydrazine as nitrogen source and it is necessary with high temperatures for the pyrolisis of NH_3 or N_2H_4 at the substrate surface [23]. While for MBE, the atomic nitrogen is provided from a plasma source, which can grow InGaN at a much lower temperature than MOCVD does. However, the quality of the surface morphology becomes poor with decreasing growth temperature due to the lower surface mobility of the adatoms [27].

The x-ray absorption spectroscopy (XAS) provides a powerful tool to investigate the structure of materials [28-31]. X-ray absorption fine structure (XAFS) encompasses both the x-ray absorption near-edge structure (XANES) and extended (EXAFS). EXAFS can describe the species of neighboring atoms and the structural environment around a selected species atom; XANES can interpret the electronic structure of the selected atom with the neighboring atoms. In this work, two high indium $In_XGa_{1-}XN$ films were investigated using synchrotron radiation experiments.

2. Experiment

Two high In InGaN samples presented here were grown by a plasma-assisted MBE system with conventional Knudsen cells for metal sources and a radio frequency plasma source for active nitrogen species. The InGaN allows were grown on the Ga-polar GaN/Sapphire templates grown by MOCVD. X-ray diffraction (XRD) reciprocal space mapping (RSM), surface morphology, hall effect and photoluminescence (PL) measurements of this two samples were detail presented in Ref. [32]. XAFS experiments were measured at National Synchrotron Radiation Research Center (NSRRC), Hsinchu, Taiwan, beamline 01C for the In *K*-edge, beamline 16A for the In *L*-edge and beamline 20A for N *K*-edge measurements, respectively, the X-ray direction is perpendicular to surface of samples. The IFEFFIT program [33] is used to fit the experimental EXAFS spectra in this paper.

3. Results and Analysis

3.1. In *K*-edge XAFS Spectra

Two InGaN samples were grown with different composition of In, x=0.78 and 0.86. The XAFS absorption spectra were measured using fluorescence yield. The incident photon direction was perpendicular to surface of the samples. In *K*-edge XAFS of samples versus the photon energy of the x-ray are shown in Figure 1. It is found that the intensity of the Zn *K*-edge absorption coefficient increases with the In composition *x* increases.

XANES refers to the region of the XAFS spectrum dominated by strong photoelectron scattering that extends about 40eV above an absorption edge. XANES probes the bonding state of molecules, the conduction band of crystalline materials, and the bond orientation. The XANES spectrum results from electron dipole transitions from initial atomic orbital states with *l* character (where *l* is the electric dipole momentum of the electron) to final states in the conduction band (or to states of antibonding molecular orbitals in the case of molecules) with $l \pm 1$ character. In the case of crystalline solids, the XANES spectrum depends on the material and the local symmetry around the central absorbing atom. In Figure 1, the features of In K-edge XANES spectra are attributed to electron excitations from In 1s to empty $5p_\pi$ (along c axis) and $5p_\sigma$ (along the bilayer) states.

XANES refers to the region of the XAFS spectrum dominated by strong photoelectron scattering that extends about 40eV above an absorption edge. XANES probes the bonding state of molecules, the conduction band of crystalline materials, and the bond orientation. The

XANES spectrum results from electron dipole transitions from initial atomic orbital states with *l* character (where *l* is the electric dipole momentum of the electron) to final states in the conduction band (or to states of antibonding molecular orbitals in the case of molecules) with *l* ± 1 character. In the case of crystalline solids, the XANES spectrum depends on the material and the local symmetry around the central absorbing atom. In Figure 1, the features of In K-edge XANES spectra are attributed to electron excitations from In 1s to empty $5p_{\pi}$ (along c axis) and $5p_{\sigma}$ (along the bilayer) states.

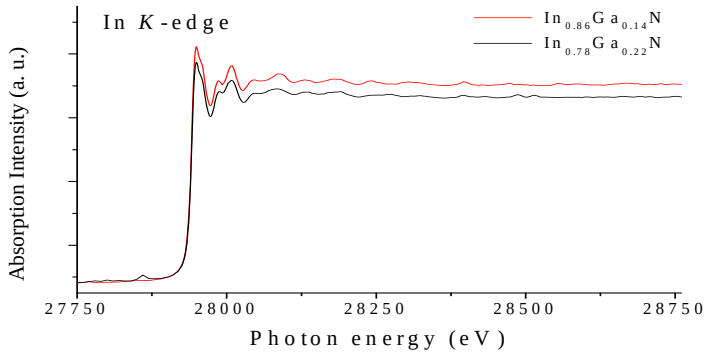

Figure 1. (Color Online) Zn *K*-edge Absorption Coefficient Plotted Versus the Photon Energy of the X-ray.

Normalized and background subtracted In *K*-edge EXAFS spectra $k^2\chi(k)$ for the two samples are shown in Figure 2 with color lines. Fitting results of the spectra $k^2\chi(k)$ are not shown in Figure 2 by using the EXAFS fitting package IFEFFIT.

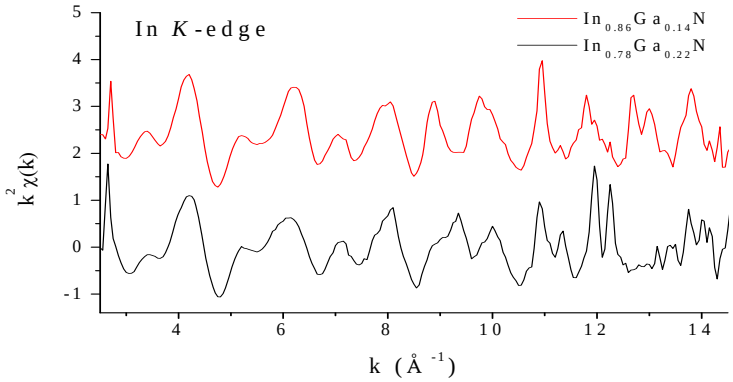

Figure 2. (Color online) k^2-weighted In K-edge EXAFS Spectra Plotted for Variable X of InGaN.

The magnitudes of Fourier transforms computed over the *k* range from ~3 to ~12 $Å^{-1}$ of the spectra $k^2\chi(k)$ are shown in Figure 3 and Figure 4 with black line. The effects of increasing In content are clearly seen. For all samples, there is little change in either the nearest neighbor In-N peak position or amplitude. To extract the bond length information, a structural model based on the InN wurtzite structure was building using the package IFEFFIT. Fitting results of the Fourier transforms are shown in Figure 3 with red line, and in good agreement with the measurement. The detail information of fitting results are shown in Table 1. R_{In-N} is denoted the distance of the In atom to the nearest neighboring N atom, i.e. bond length of In-N. The data of R_{In-N} demonstrate that the bond length of In-N decreases with composition *x* increase, this conclusion is reasonably.

Table 1. Detail Information of Fitting Results from Figure 3.

Sample	R_{In-N} [Å]
$In_{0.78}Ga_{0.22}N$	2.141
$In_{0.86}Ga_{0.14}N$	2.143

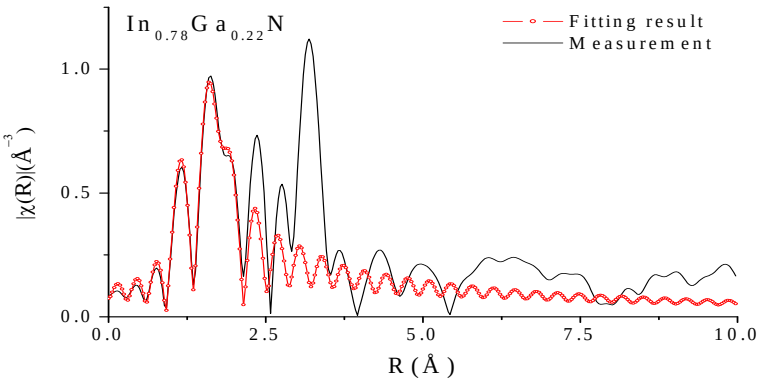

Figure 3. (Color Online) Magnitude of the Fourier Transforms of $k^2\chi(k)$ EXAFS Spectra of $In_{0.78}Ga_{0.22}N$.

The magnitudes of Fourier transforms computed over the *k* range from ~3 to ~12 Å^{-1} of the spectra $k^2\chi(k)$ are shown in Figure 3 and Figure 4 with black line. The effects of increasing In content are clearly seen. For all samples, there is little change in either the nearest neighbor In-N peak position or amplitude. To extract the bond length information, a structural model based on the InN wurtzite structure was building using the package IFEFFIT. Fitting results of the Fourier Transforms are shown in Figure 3 with red line, and in good agreement with the measurement. The detail information of fitting results are shown in Table 1. R_{In-N} is denoted the distance of the In atom to the nearest neighboring N atom, i.e. bond length of In-N. The data of R_{In-N} demonstrate that the bond length of In-N decreases with composition *x* increase, this conclusion is reasonably.

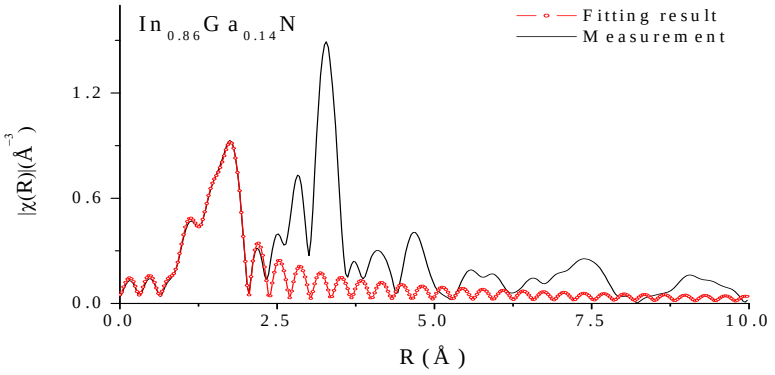

Figure 4. (Color Online) Magnitude of the Fourier Transforms of $k^2\chi(k)$ EXAFS Spectra of $In_{0.86}Ga_{0.14}N$.

3.2. *L*-edge XAFS Spectra

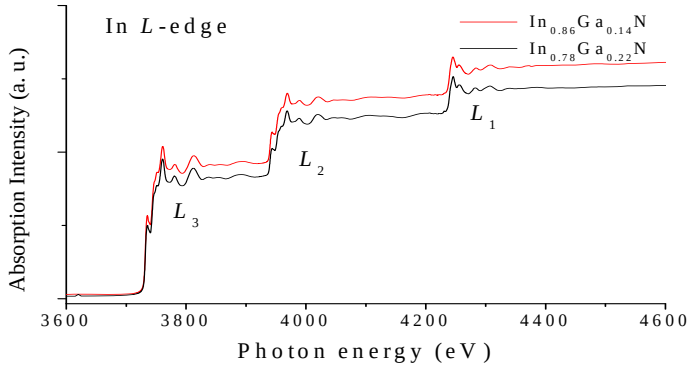

Figure 5. (Color Online)In L_1-, L_2- and L_3-edge of $In_{0.78}Ga_{0.22}N$ and $In_{0.86}Ga_{0.14}N$ at about 3720, 3970 and 4320 eV.

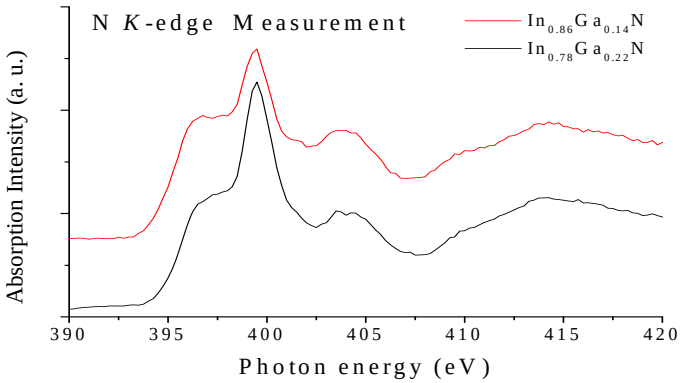

Figure 6. (Color Online) N *K*-edge of $In_{0.78}Ga_{0.22}N$ and $In_{0.86}Ga_{0.14}N$ at about 397eV.

The features of In L_1-edge XANES spectra are attributed to electron excitations form In 2*s* to 5*p*. The features of In L_2- and L_3-edge XANES spectra are associated with the transition of In $2p_{1/2}$ and $2p_{3/2}$ electrons to In 5*s* and 5*d* states. Since 5*d* orbitals are more localized than the 5*d* orbital, the transition probability of In $2p \rightarrow 5d$ can be larger than that of $2p \rightarrow 5s$. Figure 5 shows the In *L*-edge XANES spectra which are dominated by In $2p \rightarrow 5d$. The shapes of the InGaN alloys' In *L*-edge spectra were found to be nearly identical in $In_{0.78}Ga_{0.22}N$ and $In_{.086}Ga_{0.14}N$. The In *L*-edge spectra, have been normalized by the incident intensity I_0, show that the intensities of main peaks increase as the composition x increases.

3.2. *L*-edge XAFS spectra

Figure 6 shows the N *K-edge* XANES spectra (fluorescence mode) of the InGaN samples. According to the dipole-transition selection rule, the features of N *K*-edge XANES spectra are attributed to electron excitations from N 1s to empty $2p_\pi$ (along c axis) and $2p_\sigma$ (along the bilayer) states. It is found that the sharps of N *K*-edge XANES spectra have little difference between $In_{0.78}Ga_{0.22}N$ and $In_{.086}Ga_{0.14}N$.

Figure 7 shows the calculation result of N *K-edge* XANES spectra of wurtzite $In_xGa_{1-x}N$ at two composition, x=0.78 and x=0.86. The valence force field (VFF) model and FEFF code (version 9) [34] on the basis of the self-consistent-field (SCF) real-space multiple-scattering (RSMS) theory are used to calculation. For N *K-edge* calculation, a N-centered cluster of 182 atoms (radius 8.0Å) is used to calculate the SCF muffin-tin atomic potentials within the Hedin-

Lundqvist exchange potential, and a 270-atom cluster (radius 9Å) is used for the full multiple scattering (FMS) calculation. The lattice a, c and internal parameter u were assumed to be changed linearly with In composition. The XANES calculation results for high In $In_xGa_{1-x}N$ are in good agreement with the experimental spectra. Both the experimental curve peaks and shape positions are reasonably reproduced in the theoretical spectra. Based on the theoretically calculated and experimental results, it is clear that the XANES spectra can be used as the fingerpints of the composition and structure for high In InGaN

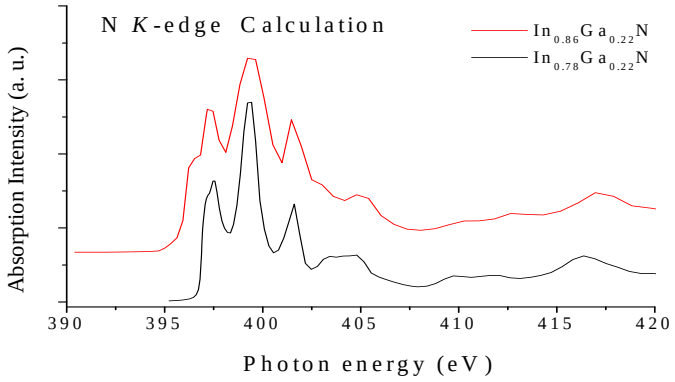

Figure 7. (Color Online) Calculation Results of N *K*-edge of $In_{0.78}Ga_{0.22}N$ and $In_{0.86}Ga_{0.14}N$.

4. Conclusion

In conclusion, we have applied synchrotron radiation to study the high In InGaN alloy films. XAFS spectra of In *K*-, L_1-, L_2- and L_3-edge and XANES spectra of N *K*-edge are obtained. In *K*-edge EXAFS data revealed the bond length of In-N and magnitudes of Fourier transforms increase with increasing of composition *x*. XANES of In *K*-, L_1-, L_2- and L_3-edge and N *K*-edge were employed to investigate the electronic structure of In and N in high In InGaN. Additionally, self-consistent-field RSMS theory calculations of N *K*-edge were performed by using FEFF 9 code. The calculation results revealed that the combination of the theoretical calculations and experiment XANES is a powerful tool for studying the electronic structure of high in InGaN alloys.

References

[1] Shuji Nakamura, Stephen Pearton and Gerhard Fasol, *The Blue Laser Diode - The Complete Story*, Springer, 2000.
[2] Zhe Chuan Feng. *Editor. III-Nitride Semiconductor Materials*, London: Imperial College Press. 2006.
[3] YL Wu, ZC. Feng, JF Lee, W Tong, BK Wagner, I Ferguson. X-ray absorption and Raman study of GaN films grown on different substrates by different techniques. *Thin Solid Films.* 2010; 518: 7475.
[4] A Kar, D Alexson, M Dutta, MA Stroscio. Evidence of compositional inhomogeneity in $In_xGa_{1-x}N$ alloys using ultraviolet and visible Raman spectroscopy. *J. Appl. Phys.* 2008; 104: 073502.
[5] BN Pantha, H Wang, N Khan, JY Lin, HX Jiang. Origin of background electron concentration in $In_xGa_{1-x}N$ alloys. *Phys. Rev. B.* 2011; 84: 075327.
[6] M César, Y Ke, W Ji, H Guo, Z Mi. Band gap of $In_xGa_{1-x}N$: A first principles analysis. *Appl. Phys. Lett.* 2011; 98: 202107.
[7] SR Meher, RVM Naidu, K Biju, A Subrahmanyam, M Jain. Carrier transport in $In_xGa_{1-x}N$ thin films grown by modified activated reactive evaporation. *Appl. Phys. Lett.* 2011; 99: 082112.
[8] ZC Feng, TR Yang, R Liu, TSA Wee. Phase separation in Zn-doped InGaN grown by metalorganic chemical vapor deposition. *Materials Science in Semiconductor Processing*. 2002; 5: 39.
[9] J Wu, W Walukiewicz, KM Yu, JW Ager III, EE Haller, H Lu, WJ Schaff. Small band gap bowing in In1−xGaxN alloys. *Appl. Phys. Lett.* 2002; 80: 4741.
[10] V Yu, Davydov, AA Klochikhin, VV Emtsev, SV Ivanov, VV Vekshin, F Bechstedt, J Furthmüller, H Harima, AV Mudryi, A Hashimoto, A Yamamoto, J Aderhold, J Graul, EE Haller. Band Gap of InN and In-Rich $In_xGa_{1-x}N$ alloys (0.36< x< 1). *Phys. Status Solidi B*. 2002, 230: R4.
[11] LW Tu, in [2].

[12] J Wu. When group-III nitrides go infrared: New properties and perspectives. *J. Appl. Phys.* 2009; 106: 011101.
[13] KY Lai, GJ Lin, YL Lai, YF Chen, JH He. Effect of indium fluctuation on the photovoltaic characteristics of InGaN/GaN multiple quantum well solar cells. *Appl. Phys. Lett.* 2010; 96: 081103.
[14] E Matioli, C Neufeld, M Iza, SC Cruz, AA Al-Heji, X Chen, RM Farrell, S Keller, S DenBaars, U Mishra, S Nakamura, J Speck, C Weisbuch. High internal and external quantum efficiency InGaN/GaN solar cells. *Appl. Phys. Lett.* 2010; 98: 021102.
[15] RH Horng, HL Hu, RC Lin, KC Peng, YC Chiang. Thermal Behavior of Sapphire-Based InGaN Light-Emitting Diodes with Cap-Shaped Copper–Diamond Substrates. *Electrochemical and Solid-State Lett.* 2011; 14: H215.
[16] M E White, KP O'Donnell, RW Martin, S Pereira, CJ Deatcher, IM Watson. Materials Science in Semiconductor Processing. 2002; B93:147.
[17] X Zhang, X Wang, H Xiao, C Yang, J Ran, C Wang, Q Hou, J Li. Simulation of $In_{0.65}Ga_{0.35}$ N single-junction solar cell. *J. Phys. D: Appl. Phys.* 2007; 40: 7335.
[18] S Hernández, R cuscó, D Pastor, L Artús, KP O'Donnell, RW Martin, IM Waston, Y Nanishi, E Calleja. Raman-scattering study of the InGaN alloy over the whole composition range. *J. Appl. Phys.* 2005; 98: 013511.
[19] ZC Feng, W Liu, SJ Chua, JW Yu, CC Yang, TR Yang, J Zhao. Photoluminescence characteristics of low indium composition InGaN thin films grown on sapphire by metalorganic chemical vapor deposition. T*hin Solid Films.* 2006; 498: 118.
[20] G Franssen, I Gorczyca, T Suski, A Kamińska, J Pereiro, E Muňoz, E Illiopoulos, A Georgakilas, SB Che, Y Ishitani, A Yoshikawa, NE Chistensen, A Svane. Bowing of the band gap pressure coefficient in InxGa1−xN alloys. *J. Appl. Phys.* 2008; 103: 033514.
[21] M Moseley, J Lowder, D Billingsley, WA Doolittle. Control of surface adatom kinetics for the growth of high-indium content InGaN throughout the miscibility gap *Appl. Phys. Lett.* 2010; 97: 191902.
[22] RR Pelá, C Caetano, M Marques, LG Ferreira, J Furthmüller, LK Teles. Accurate band gaps of AlGaN, InGaN, and AlInN alloys calculations based on LDA-1/2 approach. *Appl. Phys. Lett.* 2011; 98: 151907.
[23] A Kraus, S Hammadi, J Hisek, R Buβ, H Jönen, H Bremers, U Russow, E Sakalauskas, R Goldhahn, A Hangleiter. Growth and characterization of InGaN by RF-MBE. *J. Crystal Growth.* 2011; 323(1): 72.
[24] QX Guo, H Senda, K Saito, T Tanaka, M Nishio, J Ding, TX Fan, D Zhang, XQ Wang, ST Liu, B Shen, R Ohtani. Electronic structure of GaInN semiconductors investigated by x-ray absorption spectroscopy. *Appl. Phys. Lett.* 2011; 98: 181901.
[25] Y Huang, A Melton, B Jampana, M Jamil, JH Ryou, RD Dupuis, IT Ferguson. Compositional instability in strained InGaN epitaxial layers induced by kinetic effects. *J. Appl. Phys.* 2011; 110: 064908.
[26] I Ho, GB. Stringfellow. Solid phase immiscibility in GaInN. *Appl. Phys. Lett.* 1996; 69: 2701.
[27] X Wang, SB Che, Y Ishitani, A Yoshikawa. Effect of epitaxial temperature on N-polar InN films grown by molecular beam epitaxy. *J. Appl. Phys.* 2006; 99: 073512.
[28] QX Guo, H Senda, K Saito, T Tanaka, M Bishio, J Ding, TX Fan, D Zhang, XQ Wang, ST Liu, B Shen, R Ohtani. Effect of epitaxial temperature on N-polar InN films grown by molecular beam epitaxy. *Appl. Phys. Lett.* 2011; 98: 181901.
[29] JC Woicik, KF Ludwing Jr, TD Moustakas. Composition dependent bilayer atomic ordering in AlxGa1−xN films examined by polarization-dependent extended x-ray absorption fine structure. *Appl. Phys. Lett.* 2012; 100: 162105.
[30] CW Zhou, XD Ysn, J Han, RQ Chen, W Cao, J Metson. Study of a nitrogen-doped ZnO film with synchrotron radiation. *Appl. Phys. Lett.* 2009; 94: 171903.
[31] Sukit Limpijumnong, Jaru Jutimoosik, Nirawith Palakawong, Wantana Klysubun, Jiti Nukeaw, Mao-Hua Du, Saroj Rujirawat. Study of a nitrogen-doped ZnO film with synchrotron radiation. *Appl. Phys. Lett.* 2011; 99: 261901.
[32] ST Liu, XQ Wang, G Chen, YW Zhang, L Feng, CC. Huang, FJ Xu, N Tang, LW Sang, M Sumiya, B Shen1 Temperature-controlled epitaxy of $In_xGa_{1-x}N$ alloys and their band gap bowing. *J. Appl. Phys.* 2011; 110: 113514.
[33] B Ravel, M Newville. ATHENA, ARTEMIS, HEPHAESTUS: data analysis for X-ray absorption spectroscopy using IFEFFIT. *J. Synchrotron. Radiat.* 2005; 12: 537.
[34] AL Ankudinow, B Ravel, JJ Rehr, SD Conradson. Real-space multiple-scattering calculation and interpretation of x-ray-absorption near-edge structure. *Phys. Rev. B.* 1998; 58: 7565.